LETTERS
PUBLISHED ONLINE: 3 JUNE 2012 | DOI: 10.1038/NNANO.2012.80
nature nanotechnology

Protein–inorganic hybrid nanoflowers

Jun Ge[1,3†], Jiandu Lei[2,3†] and Richard N. Zare[3*]

Flower-shaped inorganic nanocrystals[1–3] have been used for applications in catalysis[4,5] and analytical science[6,7], but so far there have been no reports of 'nanoflowers' made of organic components[8]. Here, we report a method for creating hybrid organic–inorganic nanoflowers using copper (II) ions as the inorganic component and various proteins as the organic component. The protein molecules form complexes with the copper ions, and these complexes become nucleation sites for primary crystals of copper phosphate. Interaction between the protein and copper ions then leads to the growth of micrometre-sized particles that have nanoscale features and that are shaped like flower petals. When an enzyme is used as the protein component of the hybrid nanoflower, it exhibits enhanced enzymatic activity and stability compared with the free enzyme. This is attributed to the high surface area and confinement of the enzymes in the nanoflowers.

Hybrid organic–inorganic nanoflowers were discovered by accident when we added 0.8 mM $CuSO_4$ to phosphate buffered saline (PBS) containing 0.1 mg ml^{-1} bovine serum albumin (BSA) at pH 7.4 and 25 °C. After three days, a precipitate appeared with porous, flower-like structures. Figure 1a,b presents scanning electron microscopy (SEM) images of the nanoflowers (average size, ~3 μm), which have hierarchical structures with high surface-to-volume ratios. A transmission electron microscopy (TEM) image of a single nanoflower is shown in Fig. 1c, and Fig. 1d,e presents high-resolution TEM images of the crystal structure of one of the petals. The X-ray diffraction pattern of the nanoflower powder fits that of $Cu_3(PO_4)_2{\cdot}3H_2O$ (Supplementary Fig. S1). The morphologies of the nanoflowers were observed at different BSA concentrations decreasing from 0.5 mg ml^{-1} (NF-1, Fig. 1f) to 0.1 mg ml^{-1} (NF-2, Fig. 1g) and 0.02 mg ml^{-1} (NF-3, Fig. 1h) and were observed to mimic the growth process of flowers in nature, from small buds to blooming flowers.

SEM images as a function of time suggest the following mechanism for nanoflower self-assembly. At an early stage (step 1, Fig. 2a), primary crystals of copper phosphate are formed (Fig. 2b). At this stage, protein molecules form complexes with Cu^{2+}, predominantly through the coordination facility of amide groups in the protein backbone[9–11]. These complexes provide a location for nucleation of the primary crystals. In the second growth step (step 2, Fig. 2a), large agglomerates of protein molecules and primary crystals are formed. The kinetically controlled growth of copper phosphate crystals originates at the individual Cu^{2+} binding sites on the surfaces of the agglomerates, causing separate petals to appear (Fig. 2c). In the last stage (step 3, Fig. 2a), anisotropic growth results in complete formation of a branched flower-like structure (Fig. 2d). In this proposed growth process, the protein induces the nucleation of the copper phosphate crystals to form the scaffold for the petals and serves as a 'glue' to bind the petals together. Without the proteins, large crystals, but no nanoflowers, are formed (Supplementary Fig. S2). Calcination (350 °C) of the nanoflower made with NF-2 led to loss of the flower structure and scattered petals (Fig. 2e). Digestion of BSA by trypsin converted the nanoflowers made with NF-2 to a collapsed structure (Fig. 2f). We believe the loss or collapse of the flower structure is caused by removal of BSA from the core. The nanoflower made from NF-2 was treated with glutaraldehyde, which crosslinks the protein, followed by the addition of ethylenediaminetetraacetic acid (EDTA) to remove the Cu^{2+}. After this treatment, microspheres (average size, <2 μm) with relatively smooth surfaces were obtained (Fig. 2g), indicating that the protein is mainly located in the core of the nanoflower. SEM images of the nanoflowers treated by calcination, trypsin digestion and glutaraldehyde/EDTA were also obtained at low magnification (Supplementary Fig. S3). High-resolution SEM images (Fig. 2h,i) of the treated nanoflowers (NF-2) indicate that some BSA molecules are also present between the copper phosphate crystallites. Our evidence for this assertion is that the removal of BSA leaves some gaps between the grain boundaries, which cannot be observed on the petals of untreated nanoflowers (Fig. 2j). When 0.8 mM copper sulphate was added to a tenfold excess of phosphate buffer, immediate precipitation of copper phosphate might be expected. However, the 100-fold excess of chloride ions in PBS appears to create soluble Cu(II) chloride complexes, which retards the crystal growth process. Without chloride ions in solution, no nanoflowers were observed (Supplementary Fig. S4).

To demonstrate the generality of this method for the preparation of nanoflowers, we replaced BSA with α-lactalbumin, laccase, carbonic anhydrase and lipase. Protein-incorporated $Cu_3(PO_4)_2{\cdot}3H_2O$ nanoflowers were prepared at different protein concentrations (Fig. 3a–l). The coordination between the protein and Cu^{2+} is the main driving force for forming nanoflowers. The nitrogen atoms of the amide groups in the protein backbone and some amino-acid residues such as histidine can form complexes with Cu(II)[10,11]. Supplementary Fig. S5 shows crystal structures of α-lactalbumin[12], laccase[13], carbonic anhydrase[14] and lipase[15] with the solvent-accessible surface area of nitrogen atoms in blue. Nitrogen atoms that are accessible to ions in solvent are distributed as separate sites on the protein surface. Nucleation and growth of copper phosphate crystals originates at these Cu^{2+}-binding sites to form the separate petals, which is the key step underlying the formation of the nanoflowers. With a decreasing concentration of protein (0.5, 0.1 and 0.02 mg ml^{-1}), the number of nucleation sites decreases, resulting in nanoflowers of greater size. Figure 3 illustrates this behaviour. At the same protein concentration for a given Cu^{2+} concentration, the sizes of the different nanoflowers are similar.

Protein–inorganic nanoflowers can be demonstrated to have promising biosensor applications. Laccase is capable of oxidizing catecholamines—including epinephrine, norepinephrine and dopamine—to coloured quinone-type products detectable by colorimetric or fluorescent methods. Laccase-incorporated nanoflowers achieve more rapid oxidization of epinephrine than free laccase; indeed, in PBS (pH 6.5) containing 30 μg ml^{-1} laccase

[1]Department of Chemical Engineering, Tsinghua University, Beijing 100084, PR China, [2]National Key Laboratory of Biochemical Engineering, Institute of Process Engineering, Chinese Academy of Sciences, Beijing 100190, PR China, [3]Department of Chemistry, Stanford University, Stanford, California 94305-5080 USA; †These authors contributed equally to this work. *e-mail: zare@stanford.edu

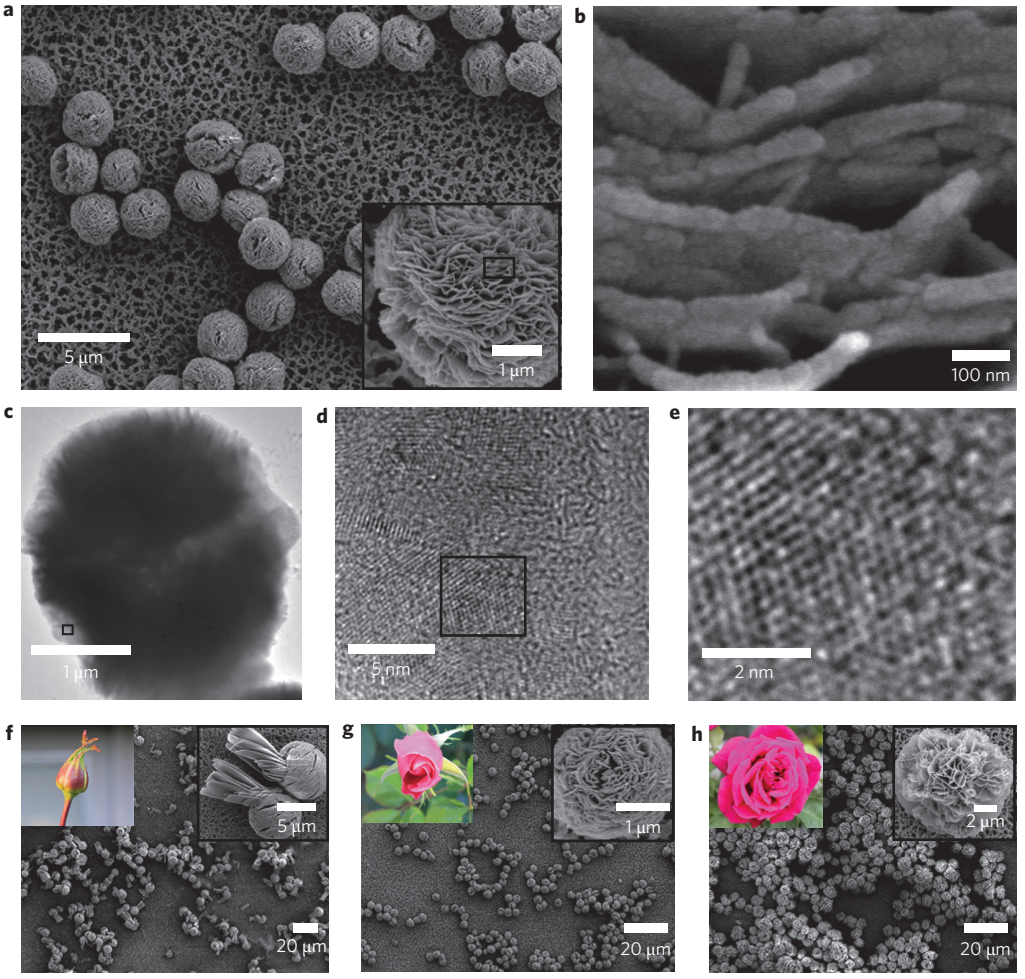

Figure 1 | Hybrid nanoflowers made from BSA and $Cu_3(PO_4)_2{\cdot}3H_2O$. a, SEM image of the nanoflowers. Inset: a single nanoflower. **b**, High-resolution SEM image of the porous structure of the petals. **c**, TEM image of the nanoflower. **d**, High-resolution TEM image of the region indicated by the square in **c**. **e**, High-resolution TEM image of the crystal lattice structure of the petal, from the square in **d**. **f**–**h**, SEM images showing the 'growth process' of the nanoflowers achieved with different concentrations of BSA: NF-1 (**f**), NF-2 (**g**), NF-3 (**h**). Insets (right): high-magnification images of the nanoflowers. To make the analogy to flowers more evident we have also provided insets (left) showing flowers in different stages of development.

and 10 μg ml^{-1} epinephrine, laccase nanoflowers can complete the oxidation of epinephrine within 10 min (in the case of free laccase this takes more than 30 min). Supplementary Fig. S6 presents the enzymatic reaction kinetics. Comparison of the initial catalytic rates in the presence of the saturated substrate shows that the enzymatic activity of the laccase nanoflower is 2.5 times higher than that of free laccase. A visual comparison of free laccase- and nanoflower-catalysed detections of epinephrine (Fig. 4a) shows a higher sensitivity when using nanoflowers. The detection range (through fluorescence of the products, Supplementary Fig. S7) reaches a diagnostic range (~0.01–1 μg ml^{-1} in 24 h urine) for epinephrine in patients with pheochromocytoma, a rare tumour of the adrenal gland[16]. Similarly, this increased activity of laccase-incorporated nanoflowers was also observed for norepinephrine (~450%) and dopamine (~480%). Moreover, on measuring its oxidative activity for epinephrine (as shown in Fig. 4b), free laccase lost 50% of its initial activity within 10 days when incubated in PBS (pH 7.4) at 25 °C, but, under the same conditions, laccase-incorporated nanoflowers maintained most of their initial activity (>95%), even after two months. The laccase nanoflower was also demonstrated to be robust in the detection of epinephrine by reusing it five times without obvious loss of activity (Supplementary Fig. S8).

Phenols are common water pollutants, most being produced from the wastewater streams of various industries. Accordingly, in another application, the oxidative coupling of phenols with 4-aminoantipyrine to form antipyrine-dyes[17] was used to evaluate the catalytic ability of the laccase-incorporated nanoflowers for the detection of phenolic compounds. Supplementary Figs S9–S11 describe the reaction kinetics. Under the same condition (25 μg ml^{-1} laccase, 10 μg ml^{-1} phenols, 0.15 mg ml^{-1} 4-aminoantipyrine at pH 6.5), the laccase-incorporated nanoflowers could convert phenols faster than free laccase (~200% for phenol, ~390% for m-cresol and ~200% for 2,4-dichlorophenol), allowing facile visible detection of these pollutants in water (Supplementary Fig. S12).

Laccase is a copper-containing oxidase, carbonic anhydrase is a zinc-containing enzyme, and lipase is a metal-free enzyme. Laccase nanoflowers exhibit ~650% increase in activity (in terms of oxidizing syringaldazine) compared with free laccase in solution. The laccase nanoflowers exhibit non-Michaelis–Menten kinetics (Supplementary Fig. S13), one possible reason for this being that the nanoscale entrapment of enzyme molecules and their interactions with Cu^{2+} in the crystals cause cooperative binding of the substrate to the active site of laccase in the nanoflowers. We also found that the carbonic anhydrase nanoflower has an increase in

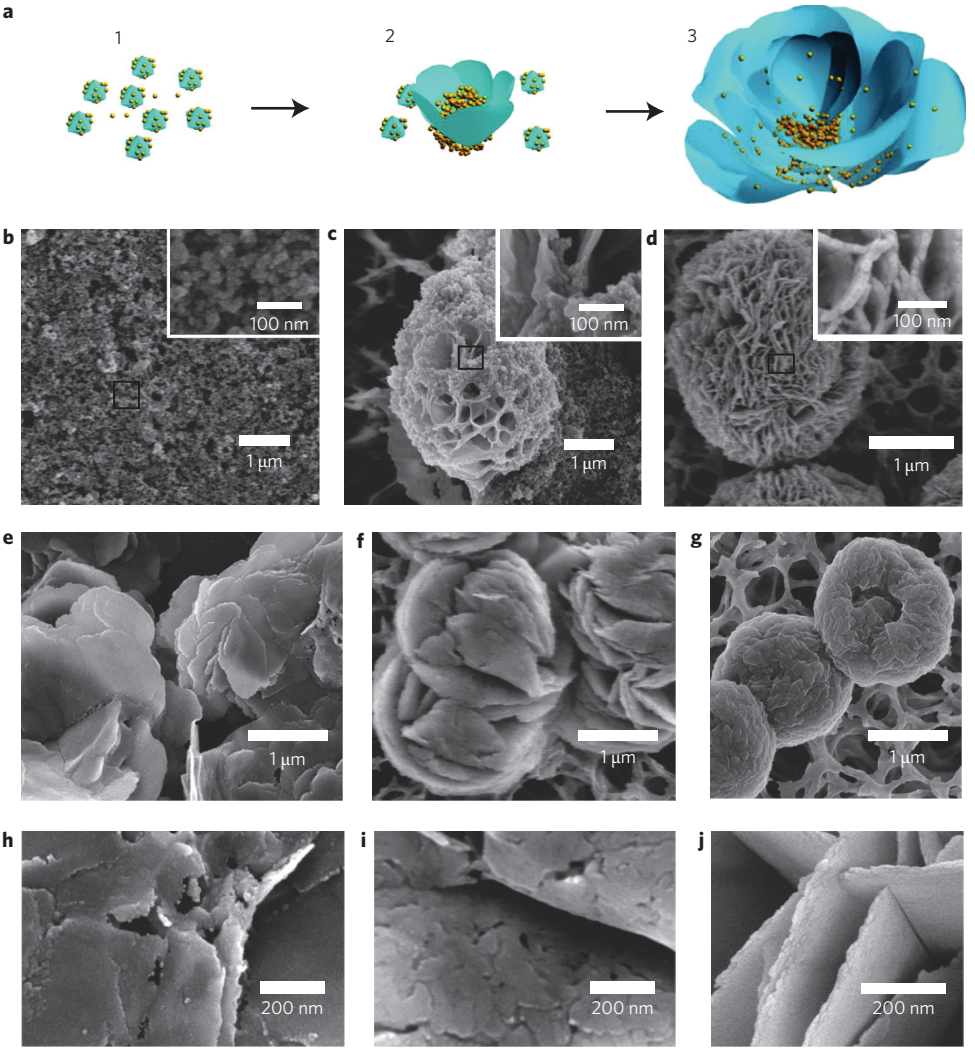

Figure 2 | Formation of BSA-incorporated $Cu_3(PO_4)_2{\cdot}3H_2O$ nanoflowers. a, Proposed mechanism, comprising three steps: (1) nucleation and formation of primary crystals; (2) growth of crystals; (3) formation of nanoflowers. Yellow spheres indicate protein molecules. **b**–**d**, SEM images at 2 h (**b**), 12 h (**c**) and 3 days (**d**). Insets: high-resolution images of the regions indicated by boxes. **e**–**g**, SEM images of nanoflowers made with NF-2, treated by calcination (**e**), trypsin (**f**) and glutaraldehyde and EDTA (**g**). **h**–**j**, High-resolution SEM images of the petals of calcined nanoflowers in NF-2 (**h**), trypsin-treated NF-2 (**i**) and in NF-2 without any treatment (**j**).

activity of ~260% compared with free enzyme in the hydration of CO_2. However, the hydrolytic activity of lipase is almost the same (~95%) after incorporation in nanoflowers when compared to the activity of free lipase.

Enzymes usually have enhanced stabilities after immobilization, but exhibit lower activities compared with free enzymes, mainly from the loss of activity during the immobilization procedure and the mass-transfer limitations in solid supports[18–21]. Single enzyme nanoparticles and nanogels represent a novel type of nanobiocatalyst with highly preserved activities[22–26]. In all the enzymes tested, the activities of single enzyme nanoparticles and nanogels could be as much as ~60–90% of those of the free enzymes. Organophosphorus hydrolase entrapped in mesoporous silica has an activity of ~200%, one of the few examples where the activity is higher than that of the free enzyme[27]. In the case of trypsin, which is a special enzyme that can digest itself, immobilization on solid supports has been shown to increase its catalytic efficiency by thousands of times compared with free trypsin in solution[28]. In comparison with the above immobilization technologies, the synthesis of enzyme nanoflowers is simple and the enhancement of enzyme stability comparable, and the activity of the nanoflowers is remarkably higher than the activities of other immobilized enzymes.

The enhanced activity of enzymes in nanoflowers probably arises from the following effects: (i) the high surface area of the nanoflower, which does not result in significant mass-transfer limitations; (ii) the cooperative effects of the nanoscale-entrapped enzyme molecules; (iii) for laccase, the interactions between laccase and the microenvironment of the nanoflower, which contains Cu^{2+} ions. (Cu^{2+} ions in nanoflowers may help to enhance laccase activity in a manner similar to when in solution[29]—the activity of free laccase was increased by a factor of 2.3 with Cu^{2+} in solution; see Supplementary Information.)

We suggest that our protein–inorganic hybrid nanoflowers might be of great interest for making various new functional protein–inorganic nanostructures, based on their enhanced activity and stability. The improved catalytic performance of the laccase-incorporated nanoflowers suggests a synergistic effect from protein and inorganic nanostructures. The protein–inorganic hybrid nanoflower, with the combined functionalities of the protein and inorganic material, is likely to have important applications in biosensors, bioanalytical devices, biofuel cells and industrial biocatalysis.

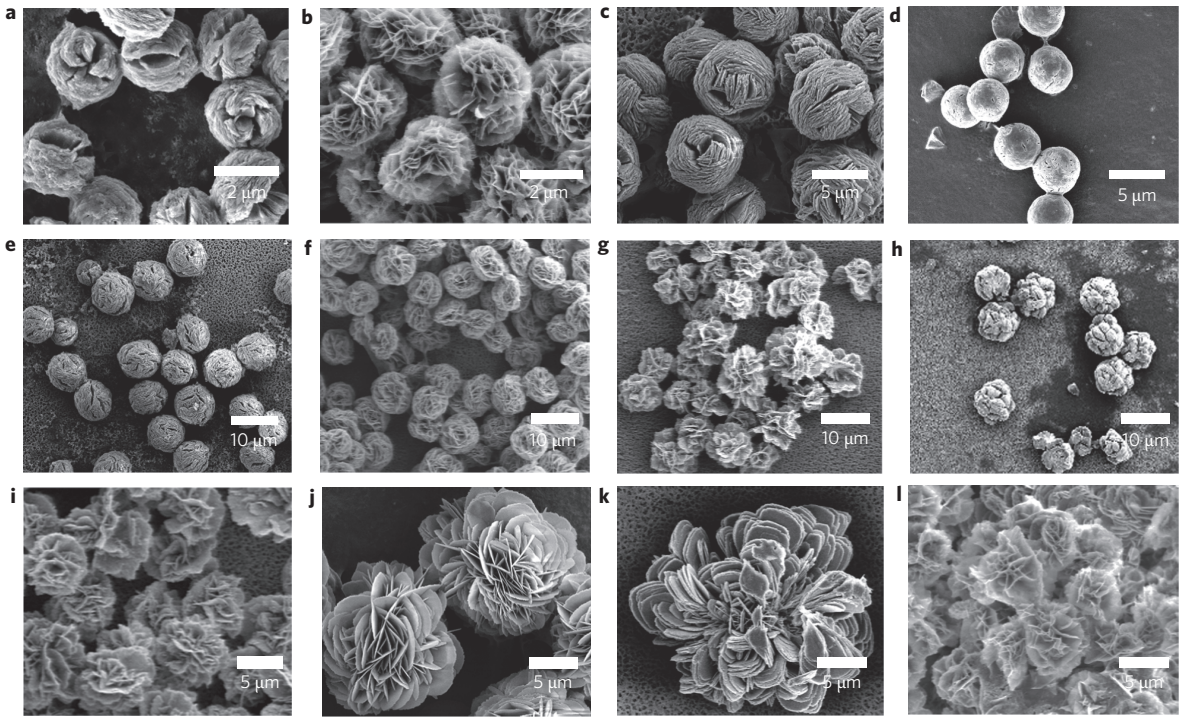

Figure 3 | SEM images of hybrid nanoflowers. a–l, Column 1, α-lactalbumin; column 2, laccase; column 3, carbonic anhydrase; column 4, lipase; at protein concentrations of 0.5 mg ml^{-1} (**a–d**), 0.1 mg ml^{-1} (**e–h**) and 0.02 mg ml^{-1} (**i–l**). From this figure the morphological changes with concentration conditions are clearly evident.

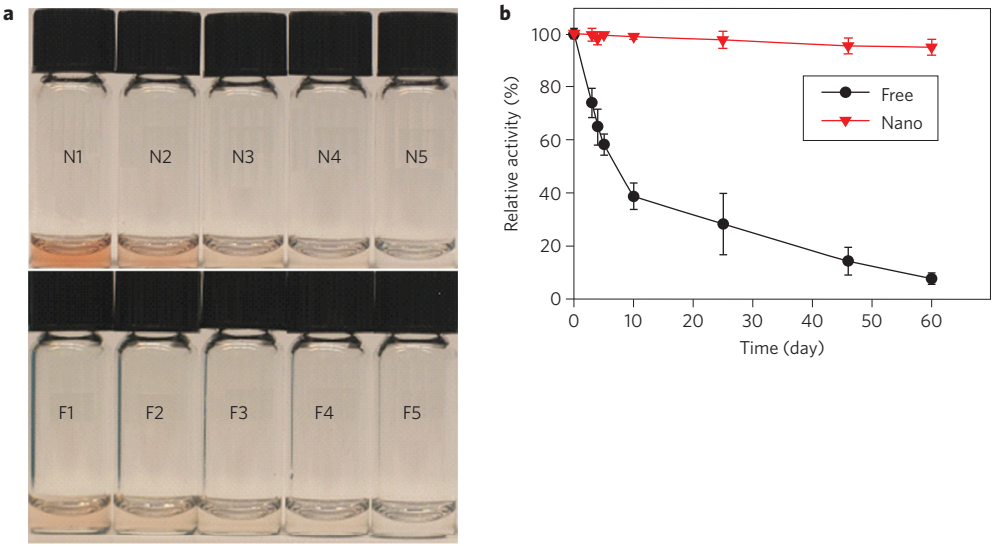

Figure 4 | Detection of epinephrine by laccase nanoflowers. a, Colour changes in epinephrine (N, laccase nanoflowers; F, free laccase; 30 μg ml^{-1} of enzyme; 25, 12.5, 5.0, 2.5, 0.25 μg ml^{-1} of epinephrine in phosphate buffer pH 6.5, denoted by 1 to 5) are clearly visible. **b**, Storage stability of laccase nanoflowers in PBS (pH 7.4) at 25 °C (Free, free laccase; Nano, laccase nanoflowers), showing that laccase nanoflowers are degraded much more slowly than free laccase over time.

Methods

For the synthesis of the protein–inorganic hybrid nanoflowers, 20 μl of aqueous $CuSO_4$ solution (120 mM) in molecular-biology-grade water was added to 3 ml of PBS (pH 7.4) containing proteins with different concentrations, followed by incubation at 25 °C for three days. For SEM analysis, the suspension of the prepared nanoflower was filtered and dried on a membrane (pore size, 0.1 μm) and sputter-coated with gold. For TEM analysis, a drop of the suspension of the prepared nanoflower was added to a carbon grid and dried at room temperature. For X-ray diffraction analysis, 20 mg of BSA was dissolved in 200 ml of PBS (pH 7.4), followed by the addition of 1.33 ml of aqueous $CuSO_4$ solution and incubation at room temperature. The nanoflower precipitate was collected, washed with deionized water, and dried at 80 °C before X-ray diffraction measurement. The protein concentration in the supernatant was measured by Bradford protein assay using BSA as standard.

Received 27 January 2012; accepted 24 April 2012; published online 3 June 2012

References

1. Song, Y. *et al.* Controlled synthesis of 2-D and 3-D dendritic platinum nanostructures. *J. Am. Chem. Soc.* **126,** 635–645 (2004).

2. Narayanaswamy, A., Xu, H., Pradhan, N., Kim, M. & Peng, X. Formation of nearly monodisperse In_2O_3 nanodots and oriented-attached nanoflowers: hydrolysis and alcoholysis vs pyrolysis. *J. Am. Chem. Soc.* **128,** 10310–10319 (2006).
3. Sun, Z. *et al.* Rational design of 3D dendritic TiO_2 nanostructures with favorable architectures. *J. Am. Chem. Soc.* **133,** 19314–19317 (2011).
4. Lim, B. *et al.* Pd–Pt bimetallic nanodendrites with high activity for oxygen reduction. *Science* **324,** 1302–1305 (2009).
5. Mohanty, A., Garg, N. & Jin, R. A universal approach to the synthesis of noble metal nanodendrites and their catalytic properties. *Angew. Chem. Int. Ed.* **49,** 4962–4966 (2010).
6. Xie, J., Zhang, Q., Lee, J. Y. & Wang, D. I. C. The synthesis of SERS-active gold nanoflower tags for *in vivo* applications. *ACS Nano* **2,** 2473–2480 (2008).
7. Jia, W., Su, L. & Lei, Y. Pt nanoflower/polyaniline composite nanofibers based urea biosensor. *Biosens. Bioelectron.* **30,** 158–164 (2011).
8. Kharisov, B. I. A review for synthesis of nanoflowers. *Recent Pat. Nanotechnol.* **2,** 190–200 (2008).
9. Harford, C. & Sarkar, B. Amino terminal Cu(II) and Ni(II)-binding (ATCUN) motif of proteins and peptides. *Acc. Chem. Res.* **30,** 123–130 (1997).
10. Smith, P. K. *et al.* Measurement of protein using bicinchoninic acid. *Anal. Biochem.* **150,** 76–85 (1985).
11. Rulíšek, L. & Vondrášek, J. Coordination geometries of selected transition metal ions (Co^{2+}, Ni^{2+}, Cu^{2+}, Zn^{2+}, Cd^{2+}, and Hg^{2+}) in metalloproteins. *J. Inorg. Biochem.* **71,** 115–127 (1998).
12. Chandra, N., Brew, K. & Acharya, K. R. Structural evidence for the presence of a secondary calcium binding site in human alpha-lactalbumin. *Biochemistry* **37,** 4767–4772 (1998).
13. Piontek, K., Antorini, M. & Choinowski, T. Crystal structure of a laccase from the fungus *Trametes versicolor* at 1.90-Å resolution containing a full complement of coppers. *J. Biol. Chem.* **277,** 37663–37669 (2002).
14. Saito, R., Sato, T., Ikai, A. & Tanaka, N. Structure of bovine carbonic anhydrase II at 1.95 Å resolution. *Acta Crystallogr. D* **60,** 792–795 (2004).
15. Ericsson, D. J. *et al.* X-ray structure of *Candida antarctica* lipase A shows a novel lid structure and a likely mode of interfacial activation. *J. Mol. Biol.* **376,** 109–119 (2008).
16. Kudva, Y. C., Sawka, A. M. & Young, W. F. Jr Clinical review 164: the laboratory diagnosis of adrenal pheochromocytoma: the Mayo Clinic experience. *J. Clin. Endocrinol. Metab.* **88,** 4533–4539 (2003).
17. Morita, E. & Nakamura, E. Solid-phase extraction of antipyrine dye for spectrophotometric determination of phenolic compounds in water. *Anal. Sci.* **27,** 489–492 (2011).
18. Kim, J., Grate, J. W. & Wang, P. Nanobiocatalysis and its potential applications. *Trends Biotechnol.* **26,** 639–646 (2008).
19. Ge, J., Lu, D., Liu, Z. X. & Liu, Z. Recent advances in nanostructured biocatalysts. *Biochem. Eng. J.* **44,** 53–59 (2009).
20. Luckarift, H. R., Spain, J. C., Naik, R. R. & Stone, M. O. Enzyme immobilization in a biomimetic silica support. *Nature Biotechnol.* **22,** 211–213 (2004).
21. Mateo, C. *et al.* Immobilization of enzymes on heterofunctional epoxy supports. *Nature Protoc.* **2,** 1022–1027 (2007).
22. Kim, J. & Grate, J. W. Single-enzyme nanoparticles armored by a nanometer-scale organic/inorganic network. *Nano Lett.* **3,** 1219–1222 (2003).
23. Yan, M., Ge, J., Liu, Z. & Ouyang, P. Encapsulation of single enzyme in nanogel with enhanced biocatalytic activity and stability. *J. Am. Chem. Soc.* **128,** 11008–11009 (2006).
24. Ge, J. *et al.* Molecular fundamentals of enzyme nanogels. *J. Phys. Chem. B* **112,** 14319–14324 (2008).
25. Ge, J., Lu, D., Wang, J. & Liu, Z. Lipase nanogel catalyzed transesterification in anhydrous dimethyl sulfoxide. *Biomacromolecules* **10,** 1612–1618 (2009).
26. Yan, M., Liu, Z. X., Lu, D. & Liu, Z. Fabrication of single carbonic anhydrase nanogel against denaturation and aggregation at high temperature. *Biomacromolecules* **8,** 560–565 (2007).
27. Lei, C., Shin, Y., Liu, J. & Ackerman, E. J. Entrapping enzyme in a functionalized nanoporous support. *J. Am. Chem. Soc.* **124,** 11242–11243 (2002).
28. Dulay, M. T., Baca, Q. J. & Zare, R. N. Enhanced proteolytic activity of covalently bound enzymes in photopolymerized sol gel. *Anal. Chem.* **77,** 4604–4610 (2005).
29. Murugesan, K., Kim, Y-M., Jeon, J-R. & Chang, Y-S. Effect of metal ions on reactive dye decolorization by laccase from *Ganoderma lucidum*. *J. Hazard. Mater.* **168,** 523–529 (2009).

Acknowledgements

The authors thank J. Brauman and K. Holmberg for helpful discussions and R-L. Jia for helping with acquiring TEM images. All experimental work was performed at Stanford University and was financially supported by the US National Science Foundation (CBET-0827806).

Author contributions

J.G., J.L. and R.N.Z. conceived and designed the experiments. J.G. and J.L. performed the experiments. J.G. and R.N.Z. analysed the data and wrote the paper.

Additional information

The authors declare no competing financial interests. Supplementary information accompanies this paper at www.nature.com/naturenanotechnology. Reprints and permission information is available online at http://www.nature.com/reprints. Correspondence and requests for materials should be addressed to R.N.Z.